Control Method of Monoinverter Dual Parallel Drive System With Interior Permanent Magnet Synchronous Machines

Yongjae Lee, *Student Member, IEEE*, and Jung-Ik Ha, *Senior Member, IEEE*

***Abstract*—This paper proposes the novel control method for a monoinverter dual parallel (MIDP) drive system with interior permanent magnet synchronous machines (IPMSMs). It includes maximum torque per ampere (MTPA) control to elevate drive efficiency and active damping control to alleviate inherent stability problem of an MIDP motor drive system. Due to the combination of reluctance and electromagnetic torques, the *d*- and *q*-axis currents of IPMSM are coupled unlike those of induction and surface-mounted permanent magnet machines. For this reason, MTPA and active damping control of a MIDP IPMSM drive system are far more complex than those with nonsalient motors. In this paper, model-based mathematical analysis about MTPA and active damping control for MIDP IPMSM drive system are provided. Experimental results with two 1.6-kW IPMSMs are presented to verify the proposed algorithm.**

***Index Terms*—Active damping, interior permanent magnet motors, maximum torque per ampere, parallel motor drives, variable speed drives.**

I. Introduction

PARALLEL-connected motor drive configurations have been researched as a cost saving solution for multimotor drive systems, such as fan, pump, electric traction, conveyor belt, and rail way propulsion. The previous studies are mainly concentrated on a parallel induction machine (IM) drive system because IM has been utilized by grid in parallel. Moreover, IM is relatively easy to control in parallel thanks to the slip [1]–[4]. As permanent magnet synchronous machines (PMSMs), however, have been widely used thanks to their high power density and efficiency, studies about dual parallel PMSM drive system which is shown in Fig. 1 were accomplished by several researchers more recently [4]–[10]. Average current control method [5], mean and differential currents control method [6], predictive control method [7], weighted current control method [4], [8], and master and slave control method [9], [10] are the representative control methods for the monoinverter dual parallel (MIDP) motor drive system.

Previous researches also proved that the current reference should be differed with the case of the typical single motor drive system [11]–[16] due to the torque difference between the motors, and they provided appropriate maximum torque per ampere (MTPA) methods for the MIDP PMSM drive system [6], [7], [10]. In [10] and [17]–[19], the instability of the MIDP PMSM configuration was presented and the active damping control method to stabilize the system was presented in [10] by Lee and Ha. They also analyzed the torque capability and low-speed instability problem of the MIDP surface-mounted PMSM (SPMSM) drive system in [17]. In [18], the singularity problem of the MIDP motor drive system is analyzed. The transfer function of parallel-connected motors is derived in [19]. Study on open-fault problem for the MIDP SPMSM drive system is also conducted by Chhun *et al*. [20].

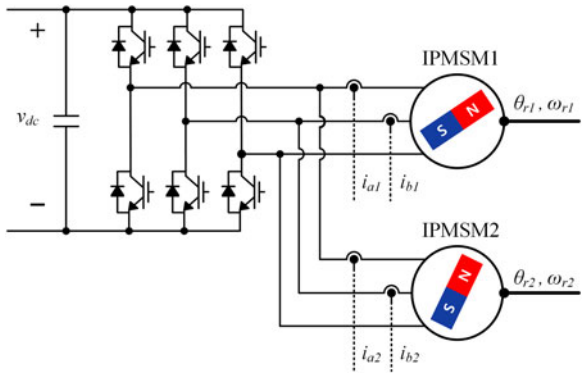

Fig. 1. Configuration of an MIDP IPMSM drive system.

All the researches about the MIDP PMSM drive system, however, have been focused on SPMSMs. It is mainly owing to the simplicity of SPMSM comes from the nonsalient structure. Especially, the nonlinear MTPA characteristic of interior PMSM (IPMSM) is considered as the biggest encumbrance as shown in Fig. 2. For this reason, it is relatively difficult to decouple the torques of the two motors in a parallel IPMSM drive system. However, IPMSMs are more widely utilized in many applications, including traction systems, thanks to their advantages, such as high efficiency, constant power speed ratio, and overload capability [21]–[26]. Thus, there has been necessity of MIDP drive system with IPMSMs.

This paper presents the control methods for the MIDP IPMSM drive system including MTPA and active damping control for the first. Proposed control methods are analyzed with the master and slave control method presented in [10]. The MTPA solution is derived for efficient drive of the MIDP IPMSM drive system and implemented using an iterative convergence method. This

Manuscript received June 10, 2015; revised August 20, 2015 and November 11, 2015; accepted December 7, 2015. Date of publication December 11, 2015; date of current version May 20, 2016. This work was supported by the Brain Korea 21 Plus Project in 2015. Recommended for publication by Associate Editor J.-I. Itoh.

The authors are with the Department of Electrical and Computer Engineering, Seoul National University, Seoul 151-744, Korea (e-mail: yongjaelee@snu.ac.kr; jungikha@snu.ac.kr).

Color versions of one or more of the figures in this paper are available online at http://ieeexplore.ieee.org.

Digital Object Identifier 10.1109/TPEL.2015.2508063

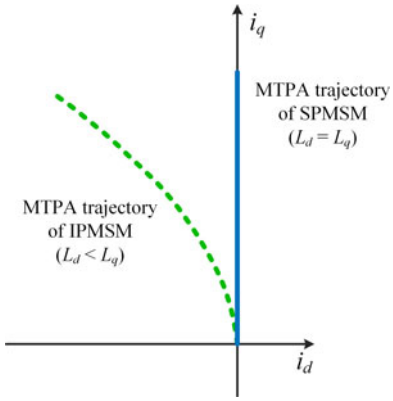

Fig. 2. MTPA trajectories of SPMSM and IPMSM.

paper proposes the decoupled active damping control method for the MIDP IPMSM drive system and examines the feasibility of the proposed active damping control through experiments.

The rest of this paper is organized as follows. Section II gives the MTPA control method for the MIDP IPMSM drive system. Section III provides the active damping control method to stabilize the system against load change or mechanical oscillation. The designed controller for the proposed system is described in Section IV. Section V gives experimental results as a verification of the proposed control methods. Finally, this paper is concluded in Section VI.

II. MTPA Control

For the MIDP SPMSM drive system, MTPA control is relatively simple because SPMSM has only electromagnetic torque which is proportional to the *q*-axis current [10]. IPMSM, however, has both of the electromagnetic and reluctance torques due to the saliency. Thus, it should be considered in the MIDP IPMSM drive system that the *d*-axis current also can produce the torque.

The terminal model of IPMSM and the torque generated by IPMSM, T_e, can be depicted as

$$\begin{bmatrix} v_{dk} \\ v_{qk} \end{bmatrix} = \begin{bmatrix} R_s & -\omega_r L_q \\ \omega_r L_d & R_s \end{bmatrix} \begin{bmatrix} i_{dk} \\ i_{qk} \end{bmatrix} + \begin{bmatrix} 0 \\ \omega_r \lambda_f \end{bmatrix} \tag{1}$$

$$T_{ek} = \frac{3}{2}\frac{n_p}{2}\left[\lambda_f + \Delta L i_{dk}\right] i_{qk} = K_t K_{ck} i_{qk} \tag{2}$$

where R_s is the phase resistance, ω_r is the electrical rotating speed, λ_f is the permanent magnet flux, L_d and L_q are the *d*- and *q*-axis inductances, i_{dk} and i_{qk} are the *d*- and *q*-axis currents, and v_{dk} and v_{qk} are the *d*- and *q*-axis voltages. Subscript *k* represents master and slave motors with 1 and 2, respectively. n_p is number of the poles, ΔL is $L_d - L_q$, K_t is $0.75\ n_p$, and K_{ck} is $\lambda_f + \Delta L i_{dk}$.

Because the two motors are connected in parallel, voltages applied to the motors are identical. It can be represented as

$$v_o^2 = v_{d1}^2 + v_{q1}^2 = v_{d2}^2 + v_{q2}^2 \tag{3}$$

TABLE I
Parameters of the Motor

Quantity	Symbol	Value	Unit
Number of pole	n_p	6	–
Phase resistance	R_s	0.55	Ω
d-axis inductance	L_d	4.27	mH
q-axis inductance	L_q	6.55	mH
Rotor flux linkage	λ_f	0.078	V · s
Rated speed	–	4000	r/min
Rated torque	–	4	N · m

where v_o is the amplitude of output voltage from inverter. It can be represented as

$$\begin{aligned} g\left(i_{d1}, i_{d2}, i_{q1}, i_{q2}\right) = {} & Z_d\left(i_{d1}^2 - i_{d2}^2\right) + Z_q\left(i_{q1}^2 - i_{q2}^2\right) \\ & + 2\omega_r R_s \Delta L\left(i_{d1} i_{q1} - i_{d2} i_{q2}\right) \\ & + 2\omega_r \lambda_f\left[\omega_r L_d\left(i_{d1} - i_{d2}\right)\right. \\ & \left. + R_s\left(i_{q1} - i_{q2}\right)\right] = 0 \end{aligned} \tag{4}$$

where $Z_d = \omega_r^2 L_d^2 + R_s^2$ and $Z_q = \omega_r^2 L_q^2 + R_s^2$. The parameters and speeds of the two motors are assumed to be identical to ease the analysis.

The MTPA current can be calculated by using the method of Lagrange multipliers and can be formulated as follows:

$$\text{Minimize} \quad i_{s1}^2 + i_{s2}^2 = i_{d1}^2 + i_{q1}^2 + i_{d2}^2 + i_{q2}^2 \tag{5}$$

$$\text{subject to} \quad \begin{cases} T_{e1} = K_t K_{c1} i_{q1} \\ T_{e2} = K_t K_{c2} i_{q2} \\ g\left(i_{d1}, i_{d2}, i_{q1}, i_{q2}\right) = 0 \end{cases}. \tag{6}$$

From (5) and (6), the Lagrange function is defined as

$$\begin{aligned} & f\left(i_{d1}, i_{q1}, i_{d2}, i_{q2}, \lambda_1, \lambda_2, \lambda_3\right) = \\ & \quad i_{d1}^2 + i_{q1}^2 + i_{d2}^2 + i_{q2}^2 + \lambda_1 g\left(i_{d1}, i_{d2}, i_{q1}, i_{q2}\right) \\ & \quad + \lambda_2\left\{T_{e1} - K_t K_{c1} i_{q1}\right\} + \lambda_3\left\{T_{e2} - K_t K_{c2} i_{q2}\right\} \end{aligned} \tag{7}$$

where λ_1, λ_2, and λ_3 are Lagrange multipliers. MTPA condition is satisfied when all partial derivatives of (7) are zero. Among the seven partial derivatives, three partial derivatives about Lagrange multiplier are identical with (6). Remained four partial derivatives can be depicted as

$$\begin{aligned} \frac{\partial f}{\partial i_{d1}} = {} & 2i_{d1} + 2\lambda_1\left[Z_d i_{d1} + R_s \Delta L \omega_r i_{q1} + L_d \lambda_f \omega_r^2\right] \\ & - \lambda_2 K_t \Delta L i_{q1} \end{aligned} \tag{8}$$

$$\begin{aligned} \frac{\partial f}{\partial i_{q1}} = {} & 2i_{q1} + 2\lambda_1\left[Z_q i_{q1} + R_s \Delta L \omega_r i_{d1} + R_s \lambda_f \omega_r\right] \\ & - \lambda_2 K_t K_{c1} \end{aligned} \tag{9}$$

$$\frac{\partial f}{\partial i_{d2}} = 2i_{d2} - 2\lambda_1 \left[Z_d i_{d2} + R_s \Delta L \omega_r i_{q2} + L_d \lambda_f \omega_r^2 \right] - \lambda_3 K_t \Delta L i_{q2} \quad (10)$$

$$\frac{\partial f}{\partial i_{q2}} = 2i_{q2} - 2\lambda_1 \left[Z_q i_{q2} + R_s \Delta L \omega_r i_{d2} + R_s \lambda_f \omega_r \right] - \lambda_3 K_t K_{c2}. \quad (11)$$

From (8)–(11), relationship between the four currents can be derived as

$$A i_{d1}^2 + B i_{d1} + C = 0 \quad (12a)$$

$$A = -\Delta L \begin{pmatrix} L_d \lambda_f^2 \omega_r^2 - \lambda_f Z_c i_{d2} + 3\lambda_f Z_d i_{d2} \\ +2\Delta L Z_d i_{d2}^2 - \Delta L Z_d i_{q2}^2 - \Delta L Z_q i_{q2}^2 \end{pmatrix} \quad (12b)$$

$$B = \lambda_f \left\{ \begin{array}{l} 2\lambda_f Z_c i_{d2} - 4\lambda_f Z_d i_{d2} - L_d \lambda_f^2 \omega_r^2 \\ -\Delta L \left[\begin{array}{l} (3Z_d - Z_c) i_{d2}^2 \\ \quad + (Z_c - 2Z_d - Z_q) i_{q2}^2 \end{array} \right] \end{array} \right\} \quad (12c)$$

$$C = \Delta L \left[\Delta L (Z_d + Z_q) i_{q1}^2 - L_d \lambda_f^2 \omega_r^2 \right] i_{d2}^2 + \left[\Delta L \lambda_f (2Z_d - Z_c + Z_q) i_{q1}^2 - L_d \lambda_f^3 \omega_r^2 \right] i_{d2} - 2\Delta L^2 Z_q i_{q1}^2 i_{q2}^2 + L_d \Delta L \lambda_f^2 \omega_r^2 \left(i_{q1}^2 + i_{q2}^2 \right) \quad (12d)$$

where $Z_c = \omega_r^2 L_d L_q + R_s^2$.

The relationship between MTPA currents can be obtained by using quadratic formula. Between the two solutions, one with minus sign gives reasonable solution for an MTPA condition. Thus, the optimal solution for the MIDP IPMSM drive system can be depicted as

$$i_{d1,\mathrm{MTPA}} = \frac{-B - \sqrt{B^2 - 4AC}}{2A}. \quad (13)$$

When it is compared to the MTPA solution of the MIDP SPMSM drive system in [10], it is much more complex due to the saliency. Fig. 3 shows the numerically achieved optimal current trajectories of the MIDP IPMSM drive system. System consists of the two 1.6-kW IPMSMs of which the parameters are listed in Table I. The rotating speed of motors are 4000 r/min and output torque of slave motor is increased from 0 to 4 N · m, while output torques of master motor in (a) and (b) are 4 and 0 N · m, respectively. For the initial state, the torque difference between the motors is positively maximum in Fig. 3(a). By injecting the negative *d*-axis current to the master motor, the positive *d*-axis current is induced to the slave motor due to the torque difference. Due to the large torque difference, each motor is operated at *R* and *S*, respectively, far from the MTPA trajectory of single IPMSM. As the torque difference is reduced, the required negative *d*-axis current on master motor is also reduced. When the output torques of two motors are identical, additional injection is not required and both motors are operated at P, MTPA point of single IPMSM. On the contrary, the positive *d*-axis current is required when the output torque of a master motor is lower than that of the slave motor, as shown in Fig. 3(b). The higher the torque difference is, the further MTPA points become from MTPA trajectory of single IPMSM.

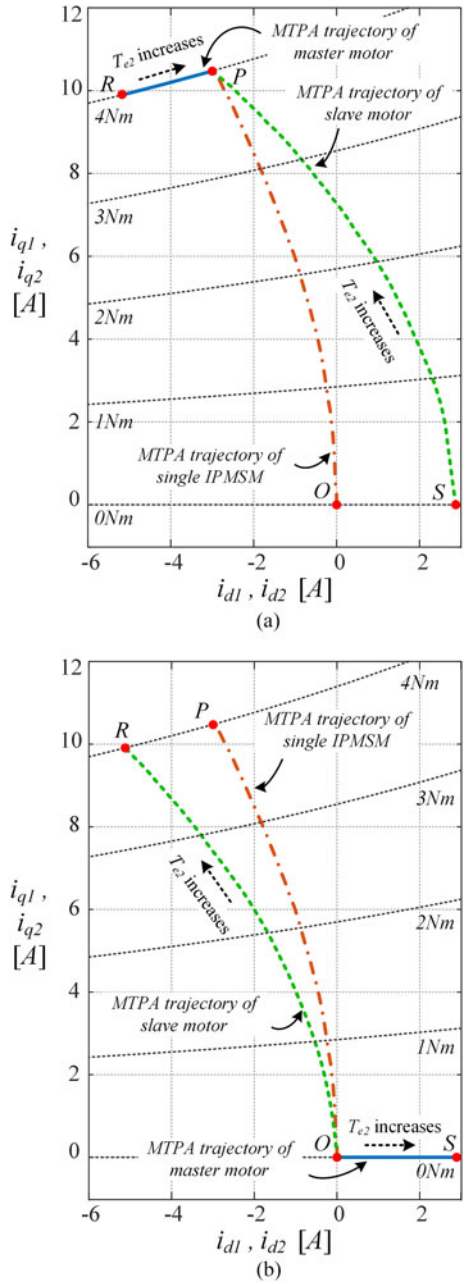

Fig. 3. MTPA trajectories of master and slave motor of the MIDP IPMSM drive system and single IPMSM according to the variance of T_{e2} from 0 to 4 N · m when T_{e1} is (a) 4 N · m and (b) 0 N · m.

Finally, these diverge from *O* to *S* and *R*, respectively. Although the MTPA trajectories of the MIDP IPMSM drive system seem like far from MTPA trajectory of a single drive system, these trajectories are the best operation points for the given operating condition.

Fig. 4 shows the root sum square of currents, i_{rss}, for three different operating methods: proposed MTPA algorithm, MTPA operation only for the master motor, and individual MTPA operation by two independent inverters. The conditions are same with that treated in Fig. 3. As shown in Fig. 4, i_{rss} of the MIDP motor drive system is higher than that of the individual drive system because MTPA operation of each motor is not secured.

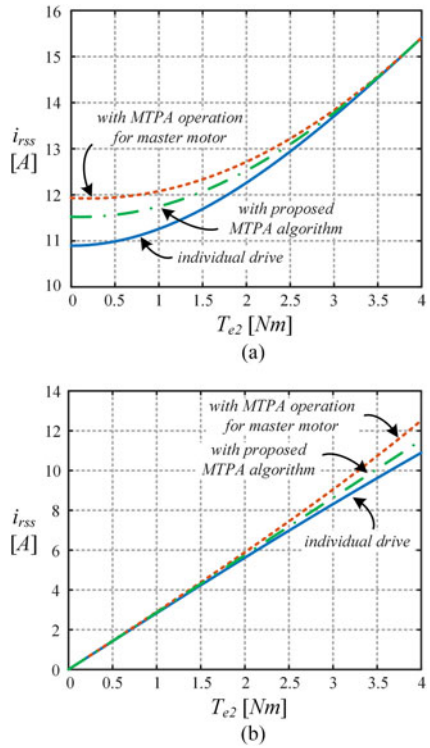

Fig. 4. $i_{\rm rss}$ according to the variance of T_{e2} from 0 to 4 N · m when T_{e1} is (a) 4 N · m and (b) 0 N · m.

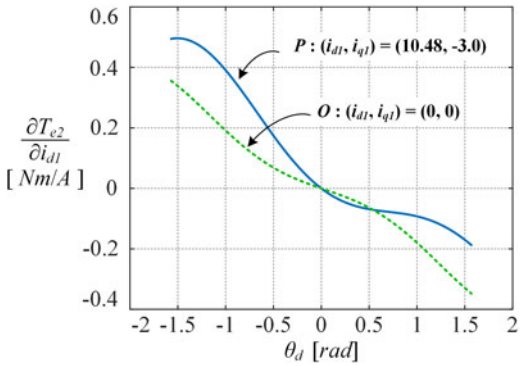

Fig. 5. Transfer functions of an active damping control.

The increments of $i_{\rm rss}$ are 5.69% and 14.78% in maximum for the graphs with and without proposed MTPA algorithm when the torque difference is maximum. As shown in the figure, output current is maximized when the rated torque is generated by both motors. Because the additional current is not required in this condition, the current rating of the inverter can be designed as two times of the conventional single motor drive system.

III. Active Damping Control

As presented in [10] and [19], parallel-connected synchronous machines suffer from inherent instability problem. System with parallel-connected synchronous machines has second-order transfer function with one zero at origin. It has very low-damping characteristic with mechanical loss. Due to the low-damping characteristic, Q-factor of the system becomes very high and overshoot is observed at resonance frequency. It can destabilize the system and break the synchronous operation. Although most of the instability problem occurs when rotating speed is close to oscillating frequency, it can happen for entire speed range due to the subharmonics and disturbance from external load. In [19], it is solved by the parallel-connected small independent inverter. In [10], active damping control using d-axis current is proposed for the MIDP SPMSM drive system. Such damping control increases the system damping coefficient and helps the system sustain synchronous state. In this section, the active damping control method for the MIDP IPMSM drive system is proposed to alleviate the instability problem.

In [10], only d-axis current is selected as control factor of the active damping control for the MIDP SPMSM drive system because d-axis current is not related to the torque generation. By eliminating extra torque to the master motor from active damping current, it is possible to decouple the torque of the master motor from active damping control. In the same manner, this paper relieves the instability of the MIDP IPMSM drive system by injecting damping current along the constant torque curve. From (2), the slope of the constant torque curve of the master motor for the given torque can be calculated as

$$\frac{\partial i_{q1}}{\partial i_{d1}} = -\frac{\Delta L i_{q1}}{K_{c1}}. \tag{14}$$

Similar to [10], the generated torque from active damping current differs according to the angle difference between two motors. Thus, the direction of the generated torque should be calculated to decide the injecting direction. For the given voltage from the inverter, the relationship between each motor voltage can be represented as

$$\begin{bmatrix} v_{d2} \\ v_{q2} \end{bmatrix} = \begin{bmatrix} \cos\theta_d & \sin\theta_d \\ -\sin\theta_d & \cos\theta_d \end{bmatrix} \begin{bmatrix} v_{d1} \\ v_{q1} \end{bmatrix} \tag{15}$$

where θ_d is electric angle difference between two motors which is defined as $\theta_2 - \theta_1$. From voltage equations of motors and (15), current relationship between two motors can be depicted as

$$\begin{aligned} \begin{bmatrix} i_{d2} \\ i_{q2} \end{bmatrix} = \cos\theta_d \begin{bmatrix} i_{d1} \\ i_{q1} \end{bmatrix} + \frac{\sin\theta_d}{Z_c} \begin{bmatrix} \omega_r R_s \Delta L & Z_q \\ -Z_d & -\omega_r R_s \Delta L \end{bmatrix} \\ \times \begin{bmatrix} i_{d1} \\ i_{q1} \end{bmatrix} - \frac{\omega_r \lambda_f}{Z_c} \left\{ (1-\cos\theta_d) \begin{bmatrix} L_q \omega_r \\ R_s \end{bmatrix} \right. \\ \left. + \sin\theta_d \begin{bmatrix} -R_s \\ L_d \omega_r \end{bmatrix} \right\}. \end{aligned} \tag{16}$$

With (14), torque variation of a slave motor by the variation of i_{d1} can be depicted as

$$\begin{aligned} \frac{\partial T_{e2}}{\partial i_{d1}} = \frac{\partial T_{e2}}{\partial i_{d2}} \left(\frac{\partial i_{d2}}{\partial i_{d1}} + \frac{\partial i_{d2}}{\partial i_{q1}} \frac{\partial i_{q1}}{\partial i_{d1}} \right) \\ + \frac{\partial T_{e2}}{\partial i_{q2}} \left(\frac{\partial i_{q2}}{\partial i_{d1}} + \frac{\partial i_{q2}}{\partial i_{q1}} \frac{\partial i_{q1}}{\partial i_{d1}} \right). \end{aligned} \tag{17}$$

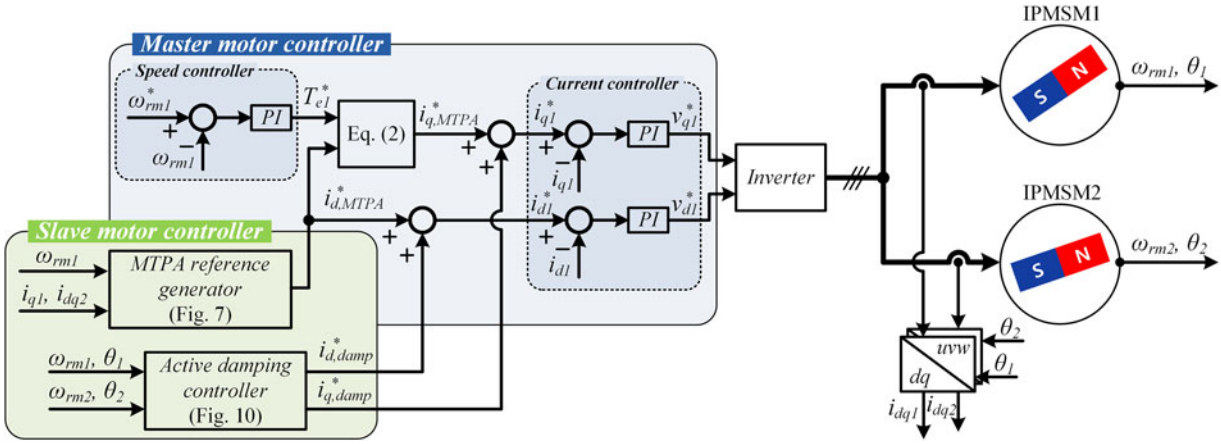

Fig. 6. Control block diagram of the proposed MIDP IPMSM drive system.

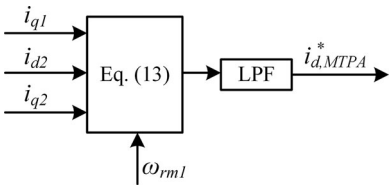

Fig. 7. MTPA reference generator.

After several mathematical arrangements, (17) can be depicted as

$$\frac{\partial T_{e2}}{\partial i_{d1}} = \alpha \sin\theta_d + \beta \sin 2\theta_d + \gamma \sin^2\theta_d + \delta\,(1-\cos\theta_d) \quad (18a)$$

$$\alpha = K_t\lambda_f\left(1 - \frac{2Z_dZ_q}{Z_c} + \frac{2\Delta L^2 R_s Z_q \omega_r}{Z_c^2 K_{c1}} i_{q1}\right) \quad (18b)$$

$$\beta = -\frac{\Delta L K_t}{Z_c}\left(\begin{array}{l} Z_d i_{d1} + \dfrac{L_q\lambda_f Z_d\omega_r^2}{Z_c} \\ +\dfrac{\Delta L Z_q}{\lambda_f + \Delta L i_{d1}} i_{q1}^2 + \dfrac{\Delta L R_s \lambda_f Z_q \omega_r}{Z_c K_{c1}} i_{q1} \end{array}\right) \quad (18c)$$

$$\gamma = -\frac{2\Delta L K_t}{Z_c^2 K_{c1}}\left[\begin{array}{l} \lambda_f Z_c Z_q i_{q1} + R_s\lambda_f^2 Z_d\omega_r \\ +2\Delta L R_s \lambda_f Z_d \omega_r i_{d1} \\ +\Delta L^2 R_s \omega_r\left(Z_d i_{d1}^2 - Z_q i_{q1}^2\right) \end{array}\right] \quad (18d)$$

$$\delta = -\Delta L \lambda_f K_t\left(\frac{Z_q}{Z_c K_{c1}} i_{q1} + \frac{R_s\omega_r}{Z_c}\right). \quad (18e)$$

In (18a), the first term is the most dominant among the four trigonometric terms in the right side. Thus, it is possible to consider that characteristic of the active damping control is similar with that of the MIDP SPMSM drive system [17]. With the parameters listed in Table I, (18a) can be illustrated as Fig. 5 when the master motor operates at *P* and *O* in Fig. 3, respectively. As shown in the figure, the graphs show the rough sinusoidal function with harmonics as expected. As depicted in (18c), amplitude of the second-order harmonic term increases as i_{q1} increases.

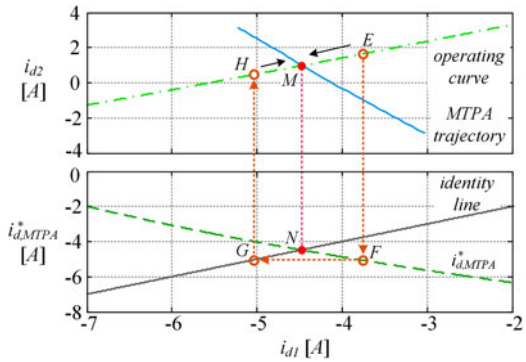

Fig. 8. Operating principle of MTPA point tracking by iterative convergence method.

For this reason, transfer function at *P* is more nonlinear than that of *O*. Nevertheless, the active damping control can be easily applied to the MIDP IPMSM drive system because the function is approximately negative sinusoidal and the sign of the function shows odd characteristic.

IV. Controller Design

The entire controller for the MIDP IPMSM drive system is shown in Fig. 6. The controller consists of a master motor controller and a slave motor controller. In the master and slave control method, speed of the master motor is controlled by the closed-loop controller. The proportional-integral (PI) regulator is adopted for the speed controller. The generated torque reference is converted to the current references based on the MTPA current reference from the MTPA reference generator. Then, the active damping currents are added to the MTPA references. The resultant current references i_{d1}^* and i_{q1}^* are also regulated by PI regulators. The generated voltage references from current controllers v_{d1}^* and v_{q1}^* are transposed to the stationary reference frame according to the angle of the master motor and modulated by an inverter.

The slave motor controller consists of the MTPA reference generator and the active damping controller. Fig. 7 shows the

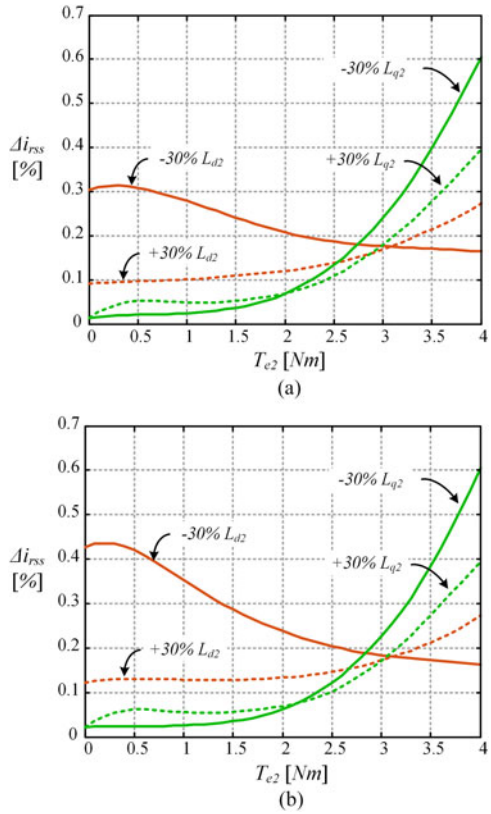

Fig. 9. $i_{\rm rss}$ error of the proposed MTPA algorithm under the $\pm 30\%$ inductance variation when $\omega_{\rm rpm}$ is (a) 4000 r/min and (b) 2000 r/min.

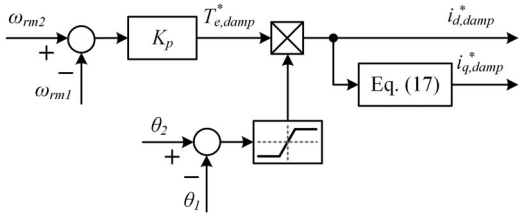

Fig. 10. Active damping controller.

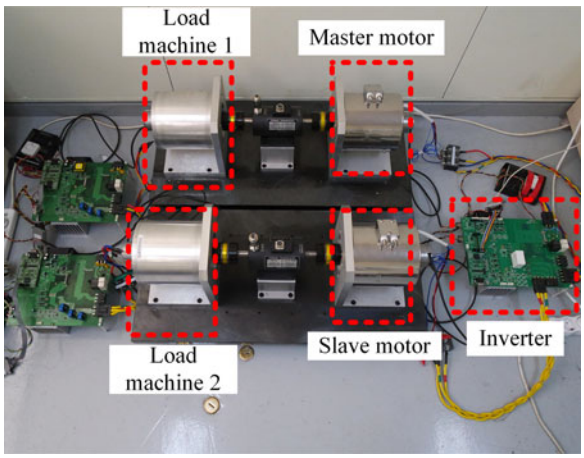

Fig. 11. Experimental setup.

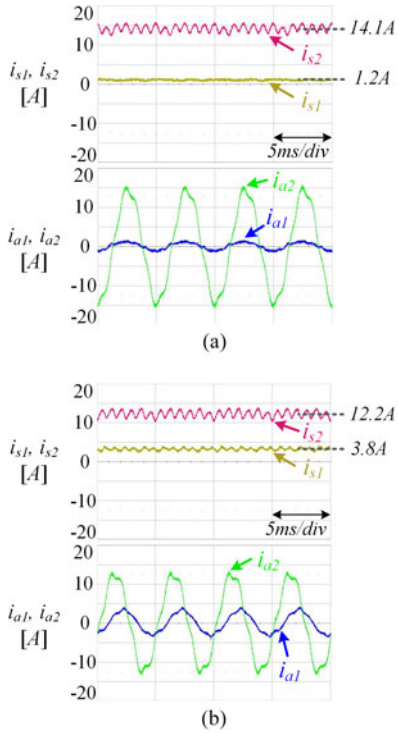

Fig. 12. Phase currents and their amplitude (a) without MTPA operation and (b) with MTPA operation.

control block diagram of MTPA reference generator. MTPA reference generator calculates $i^*_{\rm d,MTPA}$ based on i_{q1}, i_{d2}, and i_{q2} as depicted in (13). The MTPA reference generator is operated by the iterative convergence method [27]. Fig. 8 shows the principle of the proposed MTPA reference generation using iterative convergence method. Here, rotating speed is 4000 r/min and $T_{e1} = 4$ N · m. The blue solid line shows the numerically achieved MTPA trajectory on *d*-axis current plane according to the T_{e2} from 0 to 4 N · m. Although the *q*-axis currents are injected according to the torque condition, only *d*-axis currents are displayed in Fig. 8 for simple illustration. The dot dashed green line is numerically achieved operating curve when $T_{e2} =$ 2 N · m. Due to the voltage constraint, (4), operating curve for the given two torque conditions can be achieved. The dashed green line is calculation result of (13) from corresponding operating point in operating curve. The gray solid line is identity line which has unity slope. As shown in Fig. 8, *M* is the operating point where the sum current is minimized. If the system is operated at *E*, $i^*_{d,\rm MTPA}$ becomes *F* and operating point starts to move toward *H*, the corresponding operating point for *G*. As operating point moves toward *H*, *H* also moves toward *M* because corresponding $i^*_{d,\rm MTPA}$ moves toward *N*, simultaneously. When the system reaches *M*, i_{d1} of the operating point becomes consistent with corresponding $i^*_{d,\rm MTPA}$. Thus, system can stay on *M*. In this manner, system can follow MTPA point consistently.

This method has several advantages compared to the bisection method proposed in [10]. It requires much lower calculation burden despite complicate coefficients because it does not require multiple dividing operation and multiple loop calculation.

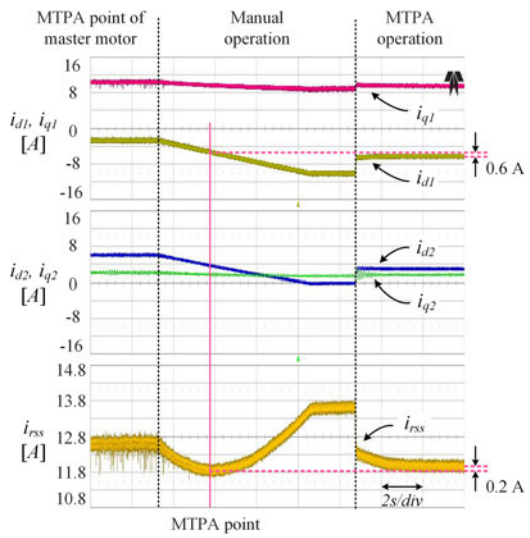

Fig. 13. Tracking performance of the proposed MTPA algorithm.

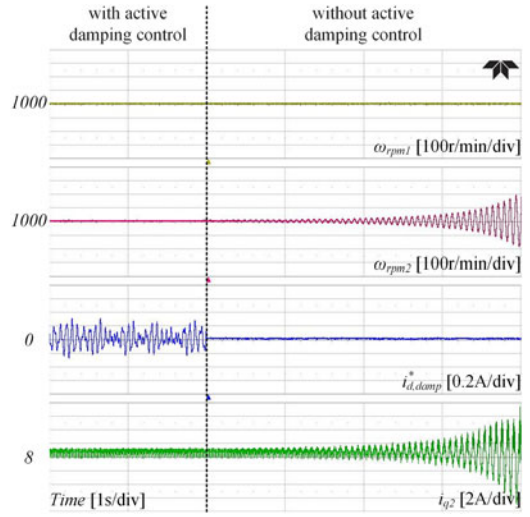

Fig. 14. Experimental result with and without active damping control.

It is also more robust to the parameter variation than the previous method because it utilizes the feedback current information from real operating curve instead of expected from parameters.

Iterative convergence method is also robust against the parameter difference between the motors. Because the proposed MTPA solution is calculated based on the assumption that the motors have same parameters, MTPA algorithm need to be robust against the parameter variations for the practical applications. Parameter variation of the proposed system can be classified into the master and slave motors. Although the parameter variation of the master motor can affect both the master motor and MTPA controller operation, it can be solved by conventional methods, such as premeasured parameter table or online parameter estimation method. Then, the parameter variation of the slave motor can be considered as parameter difference between the motors. For the analysis, the numerical analysis is accomplished for the various parameter differences ($\pm 30\%$ λ_f, R_s, L_d, L_q). Throughout the simulations, the difference of $i_{\rm rss}$ between real MTPA point and tracked point by the proposed method is negligible and lower than 1%. Fig. 9 shows the difference of $i_{\rm rss}$ between real MTPA point and tracked MTPA point under the $\pm 30\%$ inductance variation when $T_{e1} = 4\,\mathrm{N}\cdot\mathrm{m}$ and T_{e2} varies from 0 to $4\,\mathrm{N}\cdot\mathrm{m}$. Solid and dashed lines indicate the positive and negative variation, respectively. As shown in the figure, $i_{\rm rss}$ with the proposed method is almost same to the real MTPA point in spite of the 30% parameter difference, and it also shows that the proposed algorithm is robust for the various speed condition. It proves the robustness of the proposed algorithm against the various parameter variations.

Active damping controller generates active damping currents from the speed and angle information of the motor as shown in Fig. 10. It consists of proportional (P) regulator to eliminate the dc component of the output because it can deteriorate the MTPA operation. Generated damping torque reference is converted to active damping currents according to the angle difference information. As described in the previous section, output torque from the active damping current is highly related to θ_d as shown in Fig. 5. Due to the high nonlinearity, it is difficult to linearize the active damping controller. Thus, the saturation model is simply adopted as a linearization function. Although the sign function, saturation model with infinite slope, is ideal for torque generation, certain level of slope is required to prevent abrupt current changing around zero θ_d similar to [10].

Because both controllers generate current references, control frequency separation is required to prevent the interference between controllers. The fast dynamics are not essential for MTPA operation but for active damping control to suppress high-frequency oscillation and torque disturbance. To satisfy these design guidelines, LPF is applied to the MTPA reference generator to reject the high-frequency components, as shown in Fig. 7.

In our experiments, the oscillating frequency varies from 10 to 20 Hz according to the operating condition. Therefore, the cutoff frequency of the LPF is determined at 5 Hz to attenuate oscillating frequency. Because MTPA reference generator and active damping controller generate current references, current controller should can regulates the current references without phase lagging for stable operation. Thus, bandwidth of the current controller should be ten times or more high than system oscillating frequency. Control frequency also should be high enough so that current controller can have enough control bandwidth. Speed controller with low control bandwidth is also desirable to avoid the interference with the active damping controller. When the system does not have the speed sensors, speed observers are required for speed control, MTPA operation, and active damping control. Especially, the active damping control requires relatively high control bandwidth. Thus, speed observers with high bandwidth are essential for competent active damping performance.

V. Experimental Results

To verify the validity of the proposed control method for the MIDP IPMSM drive system, experiments with 1.6-kW IPMSMs are accomplished. Fig. 11 shows the experimental

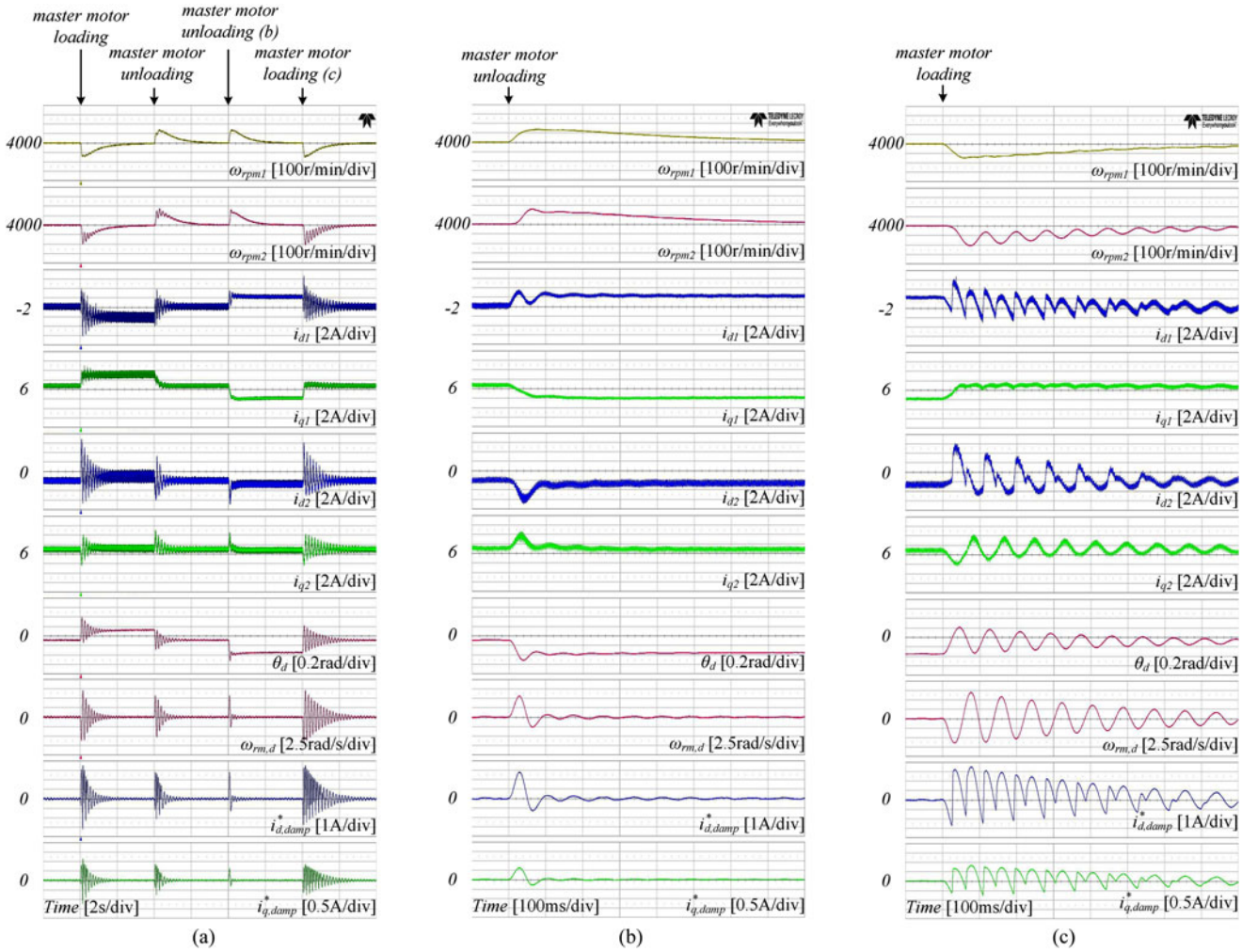

Fig. 15. Master motor step load response of the MIDP IPMSM drive system. (a) Entire sequence. (b) Zoomed waveforms of master motor step unloading and (c) restoration.

setup for demonstration. Intelligent power module PS21A7A manufactured by Mitsubishi Electric Co. is utilized as an inverter. Four ACS709 current sensors manufactured by Allegro MicroSystems, *LLC* are used to sense the phase currents of the motors. TMS320C28346 manufactured by Texas Instruments, Inc., is utilized for digital control. Inverter system is powered by dc power supply with 300 V.

Fig. 12 shows the phase currents and their amplitudes of each motor without and with MTPA operations at the rated speed. 0 and 3 N · m are loaded to master and slave motors by load machines, respectively. Due to the frictional and windage losses, actual torques generated from the test motors are higher than torques absorbed by load machines. Although the odd harmonics are contained in the current waveforms due to the harmonics in the electromotive force, the fundamental component can be compared. As displayed in Fig. 12, $i_{\rm rss}$ is reduced from 14.15 to 12.78 A thanks to the proposed MTPA operation. Although the master motor current is increased, the amplitude of the entire current is reduced because the slave motor current which takes dominant portion in the entire current is reduced. The decrement in $i_{\rm rss}$ is 9.68% for the demonstrated experimental result. As simulated in Fig. 4, decrement of $i_{\rm rss}$ is reduced as torque difference is reduced. Thus, it is possible to expect that the decrement ratio of $i_{\rm rss}$ also will be reduced for the partial-load condition.

To clearly demonstrate the accuracy and superiority of the proposed MTPA reference generating method, $i_{\rm rss}$ is measured for various operating points by sweeping current references. Fig. 13 shows the currents of each motor in the synchronous reference frame and $i_{\rm rss}$ with three current reference generating methods: MTPA operation only for the master motor, manual current sweeping, and the proposed MTPA algorithm. In this experiment, motors are regulated at the rated speed. The external loads from load machines to master and slave motors are 3 and 1 N · m, respectively. In the first stage, the master motor is controlled at MTPA point of only itself. The proposed MTPA reference generating algorithm is engaged after the manual current reference sweep to i_{d1} of -10 A. Without the proposed MTPA algorithm, i_{d1} is controlled by -2.7 A and the resultant $i_{\rm rss}$ is 12.6 A. With the proposed MTPA algorithm, i_{d1} is controlled by -6.4 A and resultant $i_{\rm rss}$ becomes 12.0 A. When it compares to the minimum $i_{\rm rss}$ point of the manual operation stage, the difference between the optimal i_{d1} and the generated i_{d1} reference from the proposed MTPA algorithm is 0.6 A and

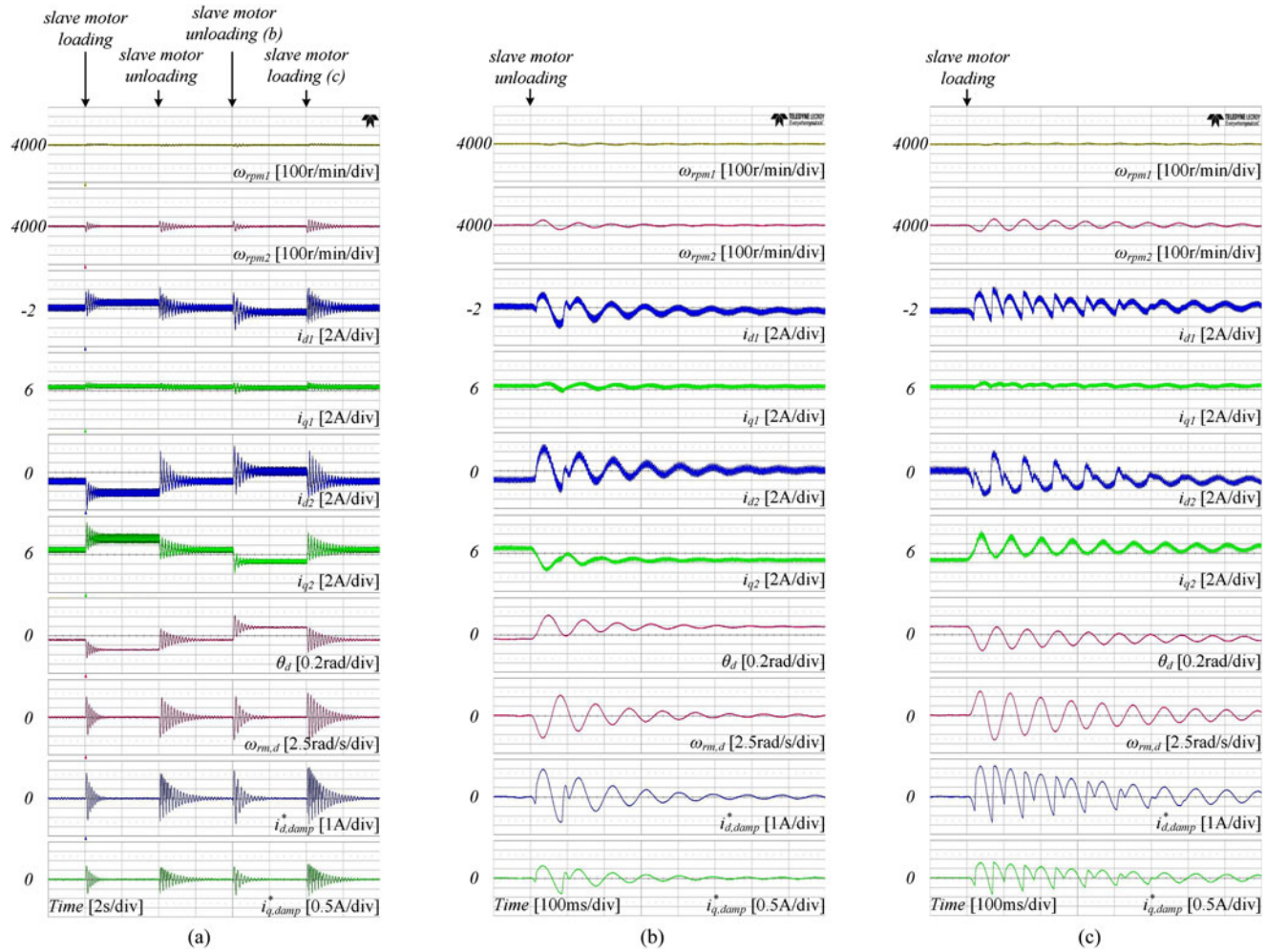

Fig. 16. Slave motor step load response of the MIDP IPMSM drive system. (a) Entire sequence. (b) Zoomed waveforms of slave motor step unloading and (c) restoration.

the difference of the resultant $i_{\rm rss}$ is 0.2 A. This calculation error comes from the parameter difference between the motors. The difference can be caused by many reasons including magnetic saturation, manufactural tolerance, and temperature difference. The further studies considering such nonideal factors should be conducted for precise MTPA operation.

Fig. 14 shows the experimental waveforms of the MIDP IPMSM drive system with and without the active damping control. The motors rotate at 1000 r/min with 3-N · m load torques. As shown in the figure, system retains the stability and constant current state thanks to the active damping control. Although only the *d*-axis damping current is depicted in the figure, the *q*-axis damping current is also injected along the constant torque curve. As soon as the active damping controller is turned off, the system started to diverge even without external load variation due to the inherent instability. Thus, it proves that the active damping control is essential to synchronize and stabilize two parallel motors.

Figs. 15 and 16 show the dynamic responses of the proposed control method against step loads. The experiments are accomplished under the rated speed and loads of 2 N · m are loaded by load machines in the nominal state. The external torque of 1 N · m is loaded and unloaded in step form for 2 s each with 2 s of the interval. The step load responses of master and slave motors are displayed in Figs. 15 and 16, respectively. Figs. 15(a) and 16(a) show the waveforms of the entire sequence and (b) and (c) of Figs. 15 and 16 show the zoomed waveforms of unloading and restoration sequence, respectively. In the steady states, the currents and angle difference are changed according to the MTPA reference generator to minimize the currents. In the transient states, the system retains the stability against the step load thanks to the active damping control. The oscillations from the underdamping characteristic of the MIDP PMSM drive system are observed [19]. The settling performance varies according to the operating condition because the characteristic of the MIDP IPMSM drive system varies according to the angle difference between the motors.

VI. Conclusion

In this paper, the control method for the MIDP IPMSM drive system is proposed. The proposed MTPA and active damping control methods for the MIDP IPMSM drive system are mathematically analyzed under the assumption of the constant and identical machine parameters. MTPA operating point of a

MIDP IPMSM drive system is derived through the method of Lagrange multipliers and implemented through iterative convergence method. The experiments verified the effectiveness and preciseness of the proposed MTPA algorithm. As shown in the experimental results, $i_{\rm rss}$ is reduced about 10% with the proposed MTPA control. The inherent instability problem in parallel-connected synchronous machines is resolved by the proposed active damping control. The active damping controller is designed through analyzing current relationship between two motors. The necessity of the active damping control and the enhanced stability of the proposed system are verified through the experiments.

REFERENCES

[1] P. M. Kelecy and R. D. Lorenz, "Control methodology for single inverter, parallel connected dual induction motor drives for electric vehicles," in *Proc. IEEE Power Electron. Spec. Conf.*, 1994, vol. 2, pp. 987–991.

[2] K. Matsuse, H. Kawai, Y. Kouno, and J. Oikawa, "Characteristics of speed sensorless vector controlled dual induction motor drive connected in parallel fed by a single inverter," *IEEE Trans. Ind. Appl.*, vol. 40, no. 1, pp. 153–161, Jan./Feb. 2004.

[3] R. Gunabalan, P. Sanjeevikumar, F. Blaabjerg, O. Ojo, and V. Subbiah, "Analysis and implementation of parallel connected two induction motor single inverter drive by direct vector control for industrial application," *IEEE Trans. Power Electron.*, vol. 30, no. 12, pp. 6472–6475, Dec. 2015.

[4] F. Xu, L. Shi, and Y. Li, "The weighted vector control of speed-irrelevant dual induction motors fed by the single inverter," *IEEE Trans. Power Electron.*, vol. 28, no. 12, pp. 5665–5672, Dec. 2013.

[5] J. M. Lazi, Z. Ibrahim, M. H. N. Talib, and R. Mustafa, "Dual motor drives for PMSM using average phase current technique," in *Proc. IEEE Int. Conf. Power Energy*, 2010, pp. 786–790.

[6] A. Del Pizzo, D. Iannuzzi, and I. Spina, "High performance control technique for unbalanced operations of single-VSI dual-PM brushless motor drives," in *Proc. IEEE Int. Ind. Electron. Symp.*, 2010, pp. 1302–1307.

[7] N. L. Nguyen, M. Fadel, and A. Llor, "A new approach to predictive torque control with dual parallel PMSM system," in *Proc. IEEE Int. Conf. Ind. Technol.*, 2013, pp. 1806–1811.

[8] A. Bouscayrol, M. Pietrzak-David, P. Delarue, R. Peña-Eguiluz, P.-E. Vidal, and X. Kestelyn, "Weighted control of traction drives with parallel-connected AC machines," *IEEE Trans. Ind. Electron.*, vol. 53, no. 6, pp. 1799–1806, Dec. 2006.

[9] D. Bidart, M. Pietrzak-David, P. Maussion, and M. Fadel, "Mono inverter multi-parallel permanent magnet synchronous motor: Structure and control strategy," *IET Electr. Power Appl.*, vol. 5, no. 3, pp. 288–294, 2011.

[10] Y. Lee and J.-I. Ha, "Control method for mono inverter dual parallel surface mounted permanent magnet synchronous machine drive system," *IEEE Trans. Ind. Electron.*, vol. 62, no. 10, pp. 6096–6107, Oct. 2015.

[11] R. Antonello, M. Carraro, and M. Zigliotto, "Maximum-torque-per-ampere operation of anisotropic synchronous permanent-magnet motors based on extremum seeking control," *IEEE Trans. Ind. Electron.*, vol. 61, no. 9, pp. 5086–5093, Sep. 2014.

[12] M. Preindl and S. Bolognani, "Optimal state reference computation with constrained MTPA criterion for PM motor drives," *IEEE Trans. Power Electron.*, vol. 30, no. 8, pp. 4524–4535, Aug. 2015.

[13] T. Sun, J. Wang, and X. Chen, "Maximum torque per ampere (MTPA) control for interior permanent magnet synchronous machine drives based on virtual signal injection," *IEEE Trans. Power Electron.*, vol. 30, no. 9, pp. 5036–5045, Sep. 2015.

[14] S. Kim, Y.-D. Yoon, S.-K. Sul, and K. Ide, "Maximum torque per ampere (MTPA) control of an IPM machine based on signal injection considering inductance saturation," *IEEE Trans. Power Electron.*, vol. 28, no. 1, pp. 488–497, Jan. 2013.

[15] S.-Y. Jung, J. Hong, and K. Nam, "Current minimizing torque control of the IPMSM using Ferrari's method," *IEEE Trans. Power Electron.*, vol. 28, no. 12, pp. 5603–5617, Dec. 2013.

[16] T. D. Do, S. Kwak, H. H. Choi, and J.-W. Jung, "Suboptimal control scheme design for interior permanent-magnet synchronous motors: An SDRE-based approach," *IEEE Trans. Power Electron.*, vol. 29, no. 6, pp. 3020–3031, Jun. 2014.

[17] Y. Lee and J.-I. Ha, "Analysis and control of mono inverter dual parallel SPMSM drive system," in *Proc. IEEE Energy Convers. Congr. Expo.*, 2014, pp. 4843–4849.

[18] J. Chiasson, D. Seto, F. Sun, A. Stankovic, and S. Bortoff, "Independent control of two PM motors using a single inverter: application to elevator doors," in *Proc. Amer. Control Conf.*, 2002, vol. 4, pp. 3093–3098.

[19] T. Nagano and J.-I. Itoh, "Parallel connected multiple drive system using small auxiliary for numbers of PMSM," in *Proc. Int. Power Electron. Conf.*, May 2014, pp. 1253–1260.

[20] L. Chhun, P. Maussion, M. Pietrzak-David, and M. Fadel, "Analysis of open-phase degradation in a mono-inverter double PMSM system," in *Proc. IEEE Annu. Conf. Ind. Electron. Soc.*, 2011, pp. 486–491.

[21] M. Zeraoulia, M. E. H. Benbouzid, and D. Diallo, "Electric motor drive selection issues for HEV propulsion systems: A comparative study," *IEEE Trans. Veh. Technol.*, vol. 55, no. 6, pp. 1756–1764, Nov. 2006.

[22] A. Vagati, G. Pellegrino, and P. Gugliemi, "Comparison between SPM and IPM motor drives for EV application," in *Proc. Int. Conf. Electr. Mach.*, Sep. 6–8, 2010, pp. 1–6.

[23] G. Pellegrino, A. Vagati, B. Boazzo, and P. Guglielmi, "Comparison of induction and PM synchronous motor drives for EV application including design examples," *IEEE Trans. Ind. Appl.*, vol. 48, no. 6, pp. 2322–2332, Nov./Dec. 2012.

[24] J. de Santiago, H. Bernhoff, B. Ekergård, S. Eriksson, S. Ferhatovic, R. Waters, and M. Leijon, "Electrical motor drivelines in commercial all-electric vehicles: A review," *IEEE Trans. Veh. Technol.*, vol. 61, no. 2, pp. 475–484, Feb. 2012.

[25] D. Matsuhashi, K. Matsuo, T. Okitsu, T. Ashikaga, and T. Mizuno, "Comparison study of various motors for EVs and the potentiality of a ferrite magnet motor," in *Proc. IEEE Power Electron. Conf.*, May 18–21, 2014, pp. 1886–1891.

[26] V. T. Buyukdegirmenci, A. M. Bazzi, and P. T. Krein, "Evaluation of induction and permanent-magnet synchronous machines using drive-cycle energy and loss minimization in traction applications," *IEEE Trans. Ind. Appl.*, vol. 50, no. 1, pp. 395–403, Jan./Feb. 2014.

[27] R. L. Burden and J. D. Faires, *Numerical Analysis*. Boston, MA, USA: Cengage Learning Inc., 2011.

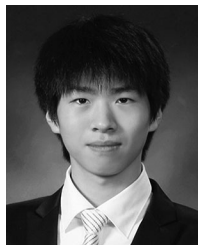

Yongjae Lee (S'12) was born in Korea in 1988. He received the B.S. and M.S. degrees in electrical engineering from Seoul National University, Seoul, Korea, in 2011 and 2013, respectively, where he is currently working toward the Ph.D. degree.

His current research interests include electric machine drives and power electronics.

Jung-Ik Ha (S'97–M'01–SM'12) was born in Korea in 1971. He received the B.S., M.S., and Ph.D. degrees in electrical engineering from Seoul National University, Seoul, Korea, in 1995, 1997, and 2001, respectively.

From 2001 to 2002, he was a Researcher with Yaskaw Electric Co., Japan. From 2003 to 2008, he was with Samsung Electronics Co., Korea, as a Senior and Principal Engineer. From 2009 to 2010, he was a Chief Technology Officer with LS Mechapion Co., Korea. Since 2010, he has been with the Department of Electrical and Computer Engineering, Seoul National University, where he is currently an Associate Professor. His research interests include circuits and control in high efficiency and integrated electric energy conversions for various industrial fields.